Highly Selective and Sensitive ~~Electrochemical~~ Molecularly Imprinting Electrochemical Sensing Platform for Bilirubin Detection in Saliva

Fatemeh Parnianchi [a], Soheila Kashanian [a,b*], Maryam Nazari [a], Carlo Santoro [c], Paolo Bollella [d], and Kambiz Varmira [e*]

[a] Faculty of Chemistry, Razi University, Kermanshah, Iran

[b] Nano Drug Delivery Research Center, Kermanshah University of Medical Sciences, Kermanshah, Iran

[c] Department of Materials Science, University of Milano-Bicocca, Via Cozzi 55, 20125 Milan, Italy

[d] Department of Chemistry and Biomolecular Sciences, Clarkson University, Potsdam, NY 13699-5810, USA

[e] Research Center of Oils and Fats, Kermanshah University of Medical Sciences, Kermanshah, Iran

*Corresponding Authors:

Soheila Kashanian: kashanian_s@yahoo.com

Kambiz Varmira: varmira@yahoo.com

Abstract

In this study, molecular imprinting polymer (MIP) was used to develop selective active sites for low-cost and easy-to-build bilirubin (BR) detection because BR is known as an indicator of liver function. When the liver does not excrete BR properly, it causes jaundice, which is associated with liver diseases, especially for in infants. High levels of BR can cause serious brain and spinal cord damage. Therefore, the identification and measurement of BR is important. In this study, for the first time, the amount of BR in saliva was identifieddetermined for the first time, which is non-invasive and cost-effective. Multi-walled carbon nanotubes (MWCNTs) were used for electrode modification before electropolymerization and MIP electrode preparation. *o*-phenylenediamine (OPD) was electropolymerized in the presence and absence of BR. The Mmodified electrodes were characterized using different techniques. The electrochemical sensor exhibited an excellent selectivity and sensitivity, notably 1.05 µA fM^{-1}. Moreover, the proposed sensor showed a wide linear range (12.08 fM to 91.81 fM) with a low detection limit of 7.80 fM. Moreover, the MIP electrode demonstrated acceptable operational stability (5% of signal loss over 10 days). After a deep characterization of the sensing platform, the MIP-modified electrode was exploited utilized for the selective detection of BR in the saliva and serum of infants.

Keywords: Molecular imprinting polymer; bilirubin; electrochemical sensor; saliva; o-phenylenediamine

Introduction

Nowadays, 80% of precocious newborns and about 50% of ordinary babies have hyperbilirubinemia ~~at~~ in their early stages of life. The bilirubin (BR) level is higher in newborns because BR cannot conjugate with glucuronic acid and remains to attach to albumin, whereas in natural hepatic mechanisms, glucuronic acid conjugates to BR and helps to excrete BR from the body [1, 2]. Hyperbilirubinemia causes body injury, thereby inspiring more researches on suitable devices for rapid detection of BR [3].

BR is produced from hemoglobin metabolism of aged red blood cells [4-6]. Almost 6 g hemoglobin is broken down every day, out of which roughly 30 mg ~~of~~ BR is produced [6-8]. BR is categorized into three main classes, two chief kinds of which exist in the human body fluids: (i) conjugated or direct BR (BR_d) and (ii) unconjugated or indirect BR (BR_i) [9, 10]. BR_i is normally present in human serum at low concentrations because it is ~~very~~ highly insoluble in water at physiological pH; therefore, its concentration is related to albumin [11, 12]. Importantly, high amounts of BR_i affect and decompose the skin and eyes [10].

The natural concentration ranges of BR_d and total BR (BR_t) in human serum are 0.8-5.1 and 3.4-17.0 μM respectively. In parallel, the physiological reference standard range of BR_t in human serum is 3.5-22.6 μM (0.2-1.3 mg/dL) [9]. A low BR level is related to anemia and coronary artery infections. High concentrations of BR may even cause biliary duct or hepatic dysfunction and ~~similarly enduring~~ brain damage and death in the highest drastic occurrences [13-15]. Hence, the BR concentration can be used as a significant guideline to recognize numerous liver diseases. High serum concentrations of BR (more than 2.5 mg/dL) in jaundice are known as hyperbilirubinemia. In the clinical laboratory, ~~generally~~ BR_d and BR_t will be generally measured as the main biomarkers for jaundice, although BR_i can be estimated from the difference between BR_d and BR_t.

A few years ago, several analytical techniques ~~were advanced for the recognition of BR~~, including enzymatic experiment [16-18], piezoelectricity [19, 20], high-performance liquid chromatography (HPLC) [21, 22], fluorimetry [23-26], chemiluminescence [27, 28], and capillary electrophoresis [29, 30]

techniques, were advanced for the recognition of BR. However, these techniques require expert operators and complex and expensive equipment. The enzymatic methods ~~showed~~ have drawbacks since they have irreproducibility and inadequate stability due to the sensitive nature of enzymes ~~nature~~ [7]. In addition, ~~there are some limitations about~~ electrochemical procedures like enzymatic electrodes, which use bilirubin oxidase (BOx) for BR detection and quantification, have some limitations. ~~These limitations include~~ such as low stability, short life span, and also high detection limit. ~~because the~~ The electrode surface and the ~~enzyme~~ active center of the enzyme have a weak electron transferring ability [31, 32]. Compared to ~~the~~ other techniques, more attention has been paid to the electrochemical sensors because of their scope of scaling down and convenient portability, simplicity, high sensitivity, and low-cost production~~, commonly without the pre-treatment of samples~~ [33]. Although many studies have been conducted on BR detection so far, using electrochemical methods for its quantitative ~~experiments~~ assessment is still ~~has~~ in its infancy~~a great way ahead~~. Electrochemical-based enzymatic methods are commonly used to detect BR. These methods are usually unstable and expensive. Among electrochemical methods, sensors that are based on the molecular imprinting of polymers are suitable alternatives. This process is able to minimize the interference of analytes with the same structure. On the other hand, it is an easy, ~~and~~ long-lasting, and cost-effective method [34].

Molecularly imprinted~~ing~~ polymer (MIP) is a polymerization method that makes it possible to synthesize semi-specific positions for targets in the molecular dimensions. ~~MIP~~ and ~~is a polymerization method that~~ uses a monomer and a target molecule ~~It makes it possible to synthesize semi-specific positions for targets in the molecular dimensions~~ [10, 35-39]. It can be prepared by electrochemical polymerization, UV polymerization, free-radical polymerization, and so on [40]. Therefore, the cavities, positions, or sites can be generated in very small sizes using a suitable matrix based on inorganic or organic materials or their combination. Template removal is the most important step; hence, the cavities with high selectivity may remain [41]. Dissimilar to the enzymes and bio-receptors, MIPs demonstrate high resistance in harsh media such as high pressures, high temperatures, and high alkaline or acidic environments. Furthermore, they can retain their analytic properties even after many years, and their stability is considerably longer than that of

biological receptors [35]. Yola et al.,~~,~~ prepared a modified electrode for ~~epinephrine~~ the selective detection of epinephrine from urine samples using an MIP sensor with a very low detection limit [42]. In another work, an MIP sensor based on polyoxometalate/carbon nitride nanotube~~s~~ composite was fabricated for the detection of organochlorine compounds ~~detection~~ with a good linear range [43].

Due to the limitations and challenges of BOx-based methods, MIPs have been used for the ~~BR~~ quantitative assay of BR. The o-phenylenediamine (OPD) electropolymerization has biocompatibility and the possibility of immobilizing different materials since it has been extensively used for the preparation of MIP sensors [44]. Polymerized OPD (PoPDA)-based compounds provide controlled-thickness polymers at the range of 10-100 nm because of the *in situ* electropolymerization, self-limiting growth, and simple~~y~~ regeneration after ~~usage~~ use [45].

Saliva is one of the most unique human body fluids for analytical experiments and analyte detection. It is noninvasive, inexpensive, easy-to-use, and stress-free. Studies have shown that certain concentrations of ions and proteins in plasma are analogous to their amounts in stimulated salivary samples [46]. The salivary glands can straightly secrete some molecules, including secretory lysozyme and immonuglobulin A (IgA), whose presence in the respective serum sample may be nil or sparse. In contrast, the BR concentration, cholesterol, lipoproteins, iron, transferrin, immunoglobuline M (IgM), and immunoglobuline G (IgG) serum levels are 4-15 times ~~more~~ greater than those seen in the saliva. This ~~proposes~~ shows that these compounds have a passive diffusion into plasma [47].

In this study, the MIP was used for the formation of selective active sites to specifically detect BR. Since multi-walled carbon nanotubes (MWCNTs) are good candidates for electrochemical applications and have been used to modify electrodes before electropolymerization and MIP electrode preparation, OPD is electropolymerized in the presence and absence of BR. MWCNTs are good choices for increasing the sensor sensitivity. In fact, the MWCNTs have a metallic behavior and ~~it~~ can ~~show~~ induce effective conductivity [11]. Then, the electrochemical measurements are performed following a precise and simple protocol in order to detect BR in real samples, including saliva and serum. For a better comparison of MIP

BR sensor, a control experiment using the non-molecularly imprinted~~ing~~ polymer (NIP) was fabricated using OPD electropolymerization in the absence of BR.

2. Experiment

2.1. Materials and reagents

N,*N*-dimethyl formamide (DMF), *o*-phenylenediamine (OPD, purity: ≥98%), dopamine, di-sodium hydrogen phosphate (Na_2HPO_4), sodium phosphate monobasic (NaH_2PO_4), sodium hydroxide (NaOH), hydrochloric acid (HCl), BR, acetonitrile, acetic acid, uric acid, and ascorbic acid were bought from Sigma–Aldrich (St. Louis, Missouri, United States). The MWCNTs were procured from the U.S. Research Nanomaterials, Inc (Houston, TX 77084, the United States). The other purifying components were bought from Merck. The Na_2HPO_4 and NaH_2PO_4 stock solutions were mixed to prepare phosphate buffer ~~solution~~ (PB) solution, and the pH values were set to the desired value through either NaOH or HCl addition. All of the solutions were prepared with double distilled water ~~of (~~Zolal Teb Shimi Company, ~~(~~Shahriar, Tehran, Iran).

2.2. Apparatus

A potentiostat Autolab PGSTAT302N-high was used to perform the electrochemical experiments, and the obtained data were analyzed by the regulator software NOVA 2.1.2. Further, three electrodes, including platinum wire, Ag/AgCl (3 M KCl) (Notably, all potentials reported in the paper are referred to as the aforementioned reference electrode), and glassy carbon electrode (GCE), were used as auxiliary, reference, and working electrodes~~,~~ respectively. The ~~S~~solutions ~~comprising of~~containing PB (0.1 M, pH 7.0), $K_3[Fe(CN)_6]/K_4[Fe(CN)_6]$ (5 mM), and KCl (0.1 M) were used during the electrochemical tests. Ehe Quanta 450 scanning electron microscope was used to investigate the surface electrode morphology ~~by~~ using the scanning electron microscopy (SEM) images (Fei Company, U.S.A.). All experimentations were carried out at room temperature.

2.3. Fabrication processes of the MIP and NIP electrodes

DMF was added to the MWCNT~~s~~ powder to prepare the MWCNT~~s~~ suspension (6 mg/2.0 mL), ~~and~~ which was then ultrasonicated for 30 min. The GCE electrode was wiped ~~by~~ with 0.05 μm alumina slurry

on a wad and washed ultrasonically with the mixture of HNO_3 and ethanol (1:1) [44]. It was then washed with ultrapure water to clean the electrode surface. After electrode drying, 10 µL of MWCNT suspension was dropped onto its surface and dried at room temperature. Acetate buffer (ABS, pH 5, 0.1 M) was utilized for the electropolymerization of the modified GCE surface by adding BR (2.0 mM) and OPD (2.0 mM). The solution was bubbled with N_2 gas before electropolymerization. Then, CV was applied at a scan rate of 50 mV s^{-1} and a potential range of 0.4-1.0 V. To remove the BR molecules, the acetonitrile-acetic acid mixture was used at room temperature for MIP electrode incubation at 5:2 ratio (v/v) for 4 min under stirring. Then, the modified electrode was investigated using electrochemical experiments. NIP/MWCNT/GCE was also fabricated under a similar situation without adding the BR to the electropolymerization step for the comparison and control experiments.

After the release~~ing~~ of the BR molecules, the electrode was washed out by ultra-pure water and was then subdued ~~to~~ for the selective recognition and rebinding tests. Rebinding of BR in the organized pits was performed by plunging the electrode in various concentrations of BR solution in 0.1 M PB (pH 7, 0.1 M) ~~beneath~~ under stirring for 10 min. In order to remove the adsorbed physical materials, the electrode was washed with distilled water.

2.4. Experimental procedure

All the electrochemical measurements were performed using ~~a~~ three-electrode configuration with MIP/MWCNT/GCE and NIP/MWCNT/GCE as working electrodes. The $[Fe(CN)_6]^{3-/4-}$ was utilized as an electrochemical probe to survey the implementation of the prepared electrodes. The electrochemical behaviors of MIP/MWCNT/GCE in the preparation procedure were characterized by electrochemical impedance spectroscopy (EIS), cyclic voltammetry (CV), and differential pulse voltammetry (DPV).

EIS evaluation was carried out at the signal amplitude of 5 mV with a regularity range of 0.01-100 000 Hz under an open-circuit voltage. The scan rate of 10 mV s^{-1} was selected for the CV recording at potentials varying from −0.5 to +0.5 V. To investigate the DPV, the potential range, step potential, modulation time, and modulation amplitude of 0.5-0.7 V, 4.0 mV, 50 ms, and 50 mV were selected respectively. All the

optimization and selectivity experiments were performed using DPV to get the best conditions for the formation of the MIP electrode surface, the modified electrode was placed in buffer and then in a buffer containing a specific concentration of BR or interfering species (in the selectivity test) and the change of current $[Fe(CN)_6]^{3-/4-}$ (ΔI) was used to assess the optimum condition. The difference between current values (ΔI) of the MIP electrode after and before re-adsorption in the solution of BR was reported [48, 49].

2.5. Diagnosis of serum and salivary BR

The ~~S~~serum and saliva samples of neonates as well as serum and saliva of healthy human were collected from Hazrat Masoumeh Hospital (Kermanshah, Iran). Breastfeeding was performed at least two hours before sampling. The serum was separated by centrifugation at 12,000 rpm for 20 minutes. The prepared samples were incubated for 30 minutes in ambient conditions and transferred to the electrochemical cell for analysis [50]. The ~~I~~individuals ~~expressed~~ gave their informed consent to participate in the study before ~~participating~~ starting the experiment, and the protocol was approved by the Medical Research Ethics Committee of the National Research Center. Every experiment was repeated ~~4~~ four times.

3. Results and discussion~~s~~

3.1. Characterization of surface morphology

The surface morphology of MIP and NIP ~~–~~modified electrodes was characterized to investigate the surface insights. As shown in Fig. 1, the structure of MIP/MWCNT/GCE compared to NIP/MWCNT/GCE is wrinkled with many small pores. According to comparisons made between MWCNT/GCE and MIP/MWCNT/GCE, we can conclude that a thin polymer is ~~placed~~ formed on the surface [51]. However, the morphology of NIP/MWCNT/GCE was much smoother than that of MIP/MWCNT/GCE, and fewer pores were found. According to Fig. 1, after removing the BR from the MIP level, cavities appeared as active binding sites for the BR molecule.

Figure 1

3.2. Electrochemical investigations

3.2.1. Electropolymerization

Fig. 2A illustrates the voltammetric cycles that have been used to produce MIP and NIP on the electrode. OPD oxidation ~~has~~ created distinct and irreversible anode peaks. In the first scan, ~~the~~ an anodic peak ~~is~~ was observed, which decrease~~d~~s with increased frequency of the consecutive scanning cycles. Fig. 2A shows the formation and growth of a polymer film in the OPD and BR. During the first cycle, an oxidation peak ~~at~~ of 0.8 V and a reduction peak of about -0.3 V ~~are~~ were observed, which result~~ed~~ in the formation of a polymer film. During polymerization, peak points ~~are~~ were formed, which ~~is~~ was probably due to the presence of -NH groups in the OPD and BR. ~~Comparing~~ The comparison of Fig. 2B and C showed~~,~~ a clear difference between MIP and NIP after polymerization and before the removal of the analyte~~, it can be seen that there is a clear difference between MIP and NIP~~. The peak corresponding to MIP ~~is~~ was smaller than the peak corresponding to NIP, which ~~is~~ was probably due to the ~~presence~~ involvement of BR analyte in the formation and growth of the polymer film. These results indicate that under these conditions a polymer film of the OPD that traps BR molecules has been ~~prepared~~ formed on the surface of the MWCNT/GCE [51]. After electropolymerization, the response to the probe redox ~~is~~ was lost due to the presence of a non-conductive film that prevent~~ed~~s the $[Fe(CN)_6]^{3-/4-}$ probe from reaching the electrode surface ~~of electrode~~.

3.2.2. Electrochemical characterization

$[Fe(CN)_6]^{3-/4-}$ probe produced an electrochemical signal in relation to the number of cavities that were not engaged by the BR molecule by reducing or oxidizing on the electrode surface. After the removal of BR by acetonitrile solution, the redox reaction was improved, indicating that BR was successfully removed from the MIP electrode surface and ~~led to~~provided greater access ~~of~~ for probe ions through the cavities in the modified layer. After incubation of MIP electrode with ~~PB~~ the analyte-containing ~~analyte~~PB, the peak currents were reduced, which indicated the blockage of some electron transfer holes for $[Fe(CN)_6]^{3-}$ and $^{/4-}$ thus proving the BR sensing features of the so prepared electrode platform. In ~~comparison~~contrast, ~~after washing and reabsorbing~~ the NIP electrode did not show any obvious change in the peak current after

washing and reabsorbing. Figs. 2B and C show a comparison between the responses of MIP and NIP electrodes. According to the voltammograms, the MIP responded~~s~~ to BR, and the NIP electrode showed~~s~~ very small changes in the current due to the lack of specific sites on the electrode surface as a result of the sensor's limited response. This feature indicates specific bonds in the MIP relative to the target molecule.

The EIS spectra (Fig. 2D) were used to investigate the properties of the electrode platform ~~at~~ in each modification step, verifying how ~~the~~ resistance to the charge transfer (R_{CT}) was changing. Fig. 2D shows the electron transfer capabilities of the modified electrode external surface. The semicircle of the EIS spectrum ~~is~~ was at greater frequencies, indicating the electron transfer procedure. Its diameter ~~is~~ was equipollent to the electron transfer resistance (R_{CT}), and its linear frequency at ~~lesser~~ lower frequencies ~~is~~ was fitted with the diffusion process. The $[Fe(CN)_6]^{3-/4-}$ probe solution ~~is~~ was used at the frequency range of 0.1-100 kHz. A comparison between diagrams A and B indicated the R_{CT} values for GCE and MWCNT/GCE were ~~calculated to be~~ 290 and 14 Ω respectively, indicating that the resistance was significantly reduced due to the MWCNT used on the electrode surface. It showed that the electrode was improved by the materials with great electrical conduction. The polymer film (OPD) created an additional barrier to electron transfer in the presence of redox probe, leading to an increase in the electron transfer resistance (R_{CT}=153 Ω). After the removal of BR, the resistance was significantly reduced (R_{CT}=58 Ω), which ~~is~~ was a sign of successful extraction of BR from the polymer. The cavities acted as an electron transfer channel and reduced the resistance. Under the observations, it can be concluded that the proposed MIP sensor has been successfully fabricated, and these observations show that the EIS spectra are consistent with the CV results.

Figure 2

3.2.3. Optimization of pH and incubation time

In order to maximize the performance of the sensor, the incubation time was optimized. The peak current decreased rapidly from minute 5 to minute 10. This process signifies the practical and rapid response of the MIP sensor to the target analyte compared to the others. Fig. 3A shows a stable response after 10 min, which indicates that the absorption has reached equilibrium and the surface is saturated. In addition,

the performance and sensitivity of the modified electrodes can be affected by the incubation time and pH of the buffer solution. Fig. 3B shows the effect of different pH values from 4 to 9 on PB. The pH 7 was selected due to ~~the~~ its high catalytic activity.

Figure 3

3.2.4. Template molecule removal behavior

The process of BR removal is a very significant step in providing suitable repeatability and high selectivity for the electrochemical sensor [52]. Different solvents can be used to extract the molecules. ~~In fact, s~~Solvents are able to swell the polymer and separate the mold molecules from the electrode surface. Among ~~the~~ various solvents, ethanol (1:1, 50% v/v), NaCl (1:1, v/v), methanol-NaOH 0.5 M (1:1, v/v), NaOH 0.5 M (1:1, v/v), acetonitrile-water (1:1, v/v), and acetonitrile-acetic acid (4:1, v/v) were used to remove the template. According to Fig. 3C, the best response appeared for the acetonitrile-acetic acid solution without any damage to the polymer after constant stirring for 5 minutes.

3.2.5. Optimization of monomer: analyte ratio and OPD polymerization scanning cycles

Fig. 4A shows the effect of different ratios of monomer and analyte onto the MIP sensor. ~~It was shown that this~~This was shown ~~is~~ to be an essential factor in the sensor response. The thickness of the polymer matrix and the amount of the formed mold ~~formed~~ are very effective factors that determine the usefulness of the MIP sensor behavior [52]. The BR concentration was optimized at 0.001 M, and this amount was used during the experimentation. According to Fig. 4A, the highest current contrast observed between different levels was 1:1. ~~At lower and higher concentrations, a~~ A decrease in the current difference was found at lower and higher concentrations, which was probably due to the large amount of monomer ~~to~~ forming the dominant molecules~~,~~ and ultimately fewer detection sites in the MIP film. During the polymerization process, the monomers are formed as a polymer film on the surface of the electrode, and the target molecules are trapped between the polymers [53]. It should be ~~added~~noted that~~,~~ the thickness of the polymer is a main parameter that affects the stability and sensitivity of the proposed sensor. Various

cycles ~~numbers~~ were performed to examine the effect of scan cycle ~~effect~~ on the polymer thickness in the range of 15-32. According to the electrode response to $[Fe(CN)_6]^{3-/4-}$ (Fig. 4B), ~~by increasing the number of scanning cycles,~~ the current response was increased to 20 cycles with an increase in the number of scanning cycles. However, when the thickness of the polymer was too high, ~~after 20 cycles,~~ it was difficult to access the molecule sites created in the polymer texture after 20 cycles, and the mass transfer resistance was increased [52]. As a result, the connection capacity was decreased.

Figure 4

3.2.6. Electrochemical behavior investigation~~s~~

The relationship between the peak current and the scan rate can determine the electrochemical mechanism on the electrode surface. Fig. 5 shows the CV peak currents of the MIP sensor at various scan rates using $[Fe(CN)_6]^{3-/4-}$ solution. The cathodic (I_{pc}) and anodic (I_{pa}) peak currents were plotted versus the scan rate square root and were expressed as I_{pc} (μA) = –0.0127 $\nu^{1/2}$ – 0.0001 (R^2 = 0.986) and I_{pa} (μA) = 0.0122 $\nu^{1/2}$ + 0.0003 (R^2 = 0.983) (where the scan rate is shown by ν with mV s^{-1} unit), suggesting ~~the~~ a typical diffusion~~–~~controlled electrochemical process.

~~Also~~Moreover, the effective surface areas of the modified electrodes were determined. For a reversible process, the following Randles-Sevcik formula was used [54, 55]:

$$I_{pa} = (2.69 \times 10^5) n^{3/2} A_0 D_0^{1/2} C_0 \nu^{1/2}$$

where I_{pa}, n, C_0, D_0, and A_0 refer to the anodic peak current, the number of transferred electrons, the concentration of $K_3[Fe(CN)_6]$, diffusion coefficient, and surface area of the electrode respectively. For 0.1 M KCl electrolyte containing 10.0 mM $K_3[Fe(CN)_6]$, $D_0 = 7.6\times10^{-6}$ cm^2 s^{-1}, and n = 1, the slope of the plot I_{pa} vs. $\nu^{1/2}$ was obtained for the modified electrodes to compute the electroactive surface area. In our experiment, the slopes of GCE~~,~~ and MIP/MWCNT/GCE were calculated, and the surface areas of these electrodes were obtained to be ≈0.11 cm^2, and ≈0.37 cm^2 respectively. The developed electrode ~~has~~ had an effective surface area that ~~is~~ was 3.3 times larger than that of the bare GCE, confirming the efficient modification of the electrode.

Figure 5

3.3. Calibration curve

Different concentrations of BR were detected using the MIP sensor after the removal of the mold in PB solution and ~~then~~ exploration of the solution containing [Fe $(CN)_6]^{3-/4-}$. The DPV technique was applied. Fig. 6 shows that the peak current decrease~~ds~~ ~~by~~ with a rise in ~~increasing~~ the BR concentration under optimal conditions, indicating that the BR molecules ~~are~~ were located in the MIP surface cavities. Using equation Y = 1.0375X + 2.878 (R^2=0.99), ~~The~~ the current response was changed linearly ~~with equation of Y = 1.0375X + 2.878 (R^2=0.99)~~. The signal-to-noise ratio of 3 was extrapolated. The graph was calculated in the range of 12.08 ~~fM to~~ 91.81 fM with a detection limit of 7.8 fM. Table 1 compares the MIP sensor with other reported methods in which the proposed sensor has an excellent and ~~an~~ optimal linear range and ~~it has~~ the lowest LOD compared to all ~~of~~ the detection methods for BR ~~in Table 1~~.

Figure 6

Table 1

3.4. Sensor selectivity

The applicability of the MIP sensor is shown by examining the interventions of molecules that have structures similar to BR. The interaction between active sites and the pattern depends on two critical factors: the size of the molecules and the functional groups of the particles. Molecules that have the same size as the target analyte have more significant interference effects. As shown in Fig. 7, the molecules progesterone, testosterone, dopamine, uric acid, and ascorbic acid were tested three times due to their structural similarity, which showed no significant effects compared to BR detection using MIP sensor.

Figure 7

3.5. Repeatability, reproducibility, and stability of the sensor

The repeatability of the OPD/MW/GCE sensor was analyzed in the 5 pM solution ~~5~~ five times using one electrode. The relative standard deviation (RSD) of the peak current was calculated to be 2.5%. The reproducibility of ~~6~~ six different modified electrodes was obtained with satisfactory results, ~~and~~ with an RSD of 3.1%. ~~Besides~~Moreover, the stability of a sensor expresses its usability when the electrode is

held for 10 days. During this period, the electrode lost only 5% of its initial response, indicating the desired stability of the proposed sensor. In comparison with other ~~works~~ studies [4, 10, 56, 57], the performance of our proposed sensor is acceptable, and it is ~~applicable~~ possible to use it several times. ~~and our~~ Our various modified MIP sensors using this fabrication have also similar responses. The RSDs of reproducibility and repeatability obtained from our proposed sensor ~~are~~ were lower ~~comparing~~than ~~to~~ those of other ~~works~~ studies [3, 39].

3.6. Analysis of serum and saliva samples of healthy humans and infants with jaundice symptoms:

~~4~~ Four electrodes were used for the analysis of saliva and serum samples. The recoveries and relative standard deviations (RSD) ~~were~~ are reported in Tables 2 and~~,~~ 3. The test results showed that the fabricated sensor ~~can~~ could report reasonable responses.

According to Table 2, the samples related to the healthy human serum and saliva were diluted and prepared in different concentrations.~~:~~ ~~then the~~ The performance of the sensor was then investigated by adding standard BR in the femtomolar range as the range of calibration curve. According to the recovery and RSD data~~,~~ indicated in Table 2, the results are acceptable.

Diagnosis of BR in neonatal saliva was performed by the proposed sensor, and the responses were compared ~~with~~ with high performance liquid chromatography (HPLC) (1260ifinity II, Agilent). ~~Also~~Further, serum samples were analyzed by the Hitachi 902 photometry and enzyme kit (Hitachi Company, Japan). According to the recovery reports of the prepared sensors (Table 3), it can be concluded that the obtained values have been reduced compared to the actual values, ~~which is~~ probably ~~related~~ due to the space barrier created by albumin in the serum and saliva, which prevents accurate measurements [58].

Table 2

Table 3

4. Conclusion

In summary, a highly selective and sensitive electrochemical sensor was developed for the first time to selectively detect BR in the saliva and serum of infants based on a simple electropolymerization polymer. The fabrication was low-cost and easy-to-build, and compounds with the same structure did not interfere with BR detection. The electrochemical sensor had an excellent wide-range of measurement (12.08 fM to 91.81 fM) with a low detection limit of 7.8 fM. AlsoMoreover, the sensitivity was calculated to be 1.05 μA fM^{-1}. Furthermore, the MIP electrode selectively sensed BR in real samples, including the saliva and serum of infants. Moreover, the MIP electrode demonstrated an acceptable stability and sensitivity over 10 days of operations.

Acknowledgments

The authors gratefully acknowledge the financial support of rResearch cCouncil of Kermanshah University of Medical Sciences (980320).

References

[1] M. Akhoundian, T. Alizadeh, G. Pan, Fabrication of the Enzyme- less Voltammetric Bilirubin Sensor Based on Sol- gel Imprinted Polymer, Electroanalysis, 32 (2020) 479-488.

[2] Z.-J. Lu, Y. Cheng, Y. Zhang, X. Wang, P. Xu, H. Yu, X. Li, Non-enzymatic Free Bilirubin Electrochemical Sensor Based on Ceria Nanocube, Sensors and Actuators B: Chemical, (2020) 129224.

[3] I. Taurino, V. Van Hoof, A. Magrez, L. Forró, G. De Micheli, S. Carrara, Efficient voltammetric discrimination of free bilirubin from uric acid and ascorbic acid by a CVD nanographite-based microelectrode, Talanta, 130 (2014) 423-426.

[4] A.-H. Wu, M.-J. Syu, Synthesis of bilirubin imprinted polymer thin film for the continuous detection of bilirubin in an MIP/QCM/FIA system, Biosensors and Bioelectronics, 21 (2006) 2345-2353.

[5] S. Karmakar, T.K. Das, S. Kundu, S. Maiti, A. Saha, Physicochemical Understanding of Protein-Bound Quantum Dot-Based Sensitive Probing of Bilirubin: Validation with Real Samples and Implications of Protein Conformation in Sensing, ACS Applied Bio Materials, (2020).

[6] R.P. Edachana, A. Kumaresan, V. Balasubramanian, R. Thiagarajan, B.G. Nair, S.B.T. Gopalakrishnan, based device for the colorimetric assay of bilirubin based on in-situ formation of gold nanoparticles, Microchimica Acta, 187 (2020) 60.

[7] H.-B. Noh, M.-S. Won, Y.-B. Shim, Selective nonenzymatic bilirubin detection in blood samples using a Nafion/Mn–Cu sensor, Biosensors and Bioelectronics, 61 (2014) 554-561.

[8] A. H Kamel, A.E.-G.E. Amr, H.R. Galal, M.A. Al-Omar, A.A. Almehizia, Screen-Printed Sensor Based on Potentiometric Transduction for Free Bilirubin Detection as a Biomarker for Hyperbilirubinemia Diagnosis, Chemosensors, 8 (2020) 86.

[9] M. Zhang, L. Xu, Q. Ma, H. Yu, H. Fang, Z. Lin, Q. Zhang, Z. Chen, A pH-controlled kit for total and direct bilirubin built on mimetic peroxidase CoFe2O4-DOPA-catalyzed fluorescence enhancement, ACS Applied Materials & Interfaces, 10 (2018) 42155-42164.
[10] M.L. Yola, C. Göde, N. Atar, Molecular imprinting polymer with polyoxometalate/carbon nitride nanotubes for electrochemical recognition of bilirubin, Electrochimica Acta, 246 (2017) 135-140.
[11] I. Taurino, V. Van Hoof, G. De Micheli, S. Carrara, Superior sensing performance of multi-walled carbon nanotube-based electrodes to detect unconjugated bilirubin, Thin Solid Films, 548 (2013) 546-550.
[12] E. Ahmmed, A. Mondal, A. Sarkar, S. Chakraborty, S. Lohar, N.C. Saha, K. Dhara, P. Chattopadhyay, Bilirubin Quantification in Human Blood Serum by Deoxygenation Reaction Switch-Triggered Fluorescent Probe, ACS Applied Bio Materials, (2020).
[13] Ç. Çiçek, F. Yılmaz, E. Özgür, H. Yavuz, A. Denizli, Molecularly imprinted quartz crystal microbalance sensor (QCM) for bilirubin detection, Chemosensors, 4 (2016) 21.
[14] W. Xiao, D. Zhi, Q. Pan, Y. Liang, F. Zhou, Z. Chen, A ratiometric bilirubin sensor based on a fluorescent gold nanocluster film with dual emissions, Analytical Methods, (2020).
[15] C. Song, Y. Li, B. Wang, Y. Hong, C. Xue, Q. Li, E. Shen, D. Cui, A novel anticoagulant affinity membrane for enhanced hemocompatibility and bilirubin removal, Colloids and Surfaces B: Biointerfaces, 197 (2020) 111430.
[16] K. Kurosaka, S. Senba, H. Tsubota, H. Kondo, A new enzymatic assay for selectively measuring conjugated bilirubin concentration in serum with use of bilirubin oxidase, Clinica chimica acta, 269 (1998) 125-136.
[17] S. Iwatani, H. Nakamura, D. Kurokawa, K. Yamana, K. Nishida, S. Fukushima, T. Koda, N. Nishimura, H. Nishio, K. Iijima, Fluorescent protein-based detection of unconjugated bilirubin in newborn serum, Scientific reports, 6 (2016) 28489.
[18] T. Kovaľ, L. Švecová, L.H. Østergaard, T. Skalova, J. Dušková, J. Hašek, P. Kolenko, K. Fejfarová, J. Stránský, M. Trundová, trp–His covalent adduct in bilirubin oxidase is crucial for effective bilirubin binding but has a minor role in electron transfer, Scientific reports, 9 (2019) 1-13.
[19] Z. Yang, J. Yan, C. Zhang, Piezoelectric detection of bilirubin based on bilirubin-imprinted titania film electrode, Analytical biochemistry, 421 (2012) 37-42.
[20] C. Zhang, W. Bai, T. Qin, Z. Yang, Fabrication of Red Mud/Molecularly Imprinted Polypyrrole-Modified Electrode for the Piezoelectric Sensing of Bilirubin, IEEE Sensors Journal, 19 (2018) 1280-1284.
[21] J. Zelenka, M. Leníček, L. Muchová, M. Jirsa, M. Kudla, P. Balaž, M. Zadinová, J.D. Ostrow, R.J. Wong, L. Vítek, Highly sensitive method for quantitative determination of bilirubin in biological fluids and tissues, Journal of Chromatography B, 867 (2008) 37-42.
[22] G. Ma, J. Lin, W. Cai, B. Tan, X. Xiang, Y. Zhang, P. Zhang, Simultaneous determination of bilirubin and its glucuronides in liver microsomes and recombinant UGT1A1 enzyme incubation systems by HPLC method and its application to bilirubin glucuronidation studies, Journal of Pharmaceutical and Biomedical Analysis, 92 (2014) 149-159.
[23] Y. Andreu, J. Galbán, S. de Marcos, J.R. Castillo, Determination of direct-bilirubin by a fluorimetric-enzymatic method based on bilirubin oxidase, Fresenius' journal of analytical chemistry, 368 (2000) 516-521.

[24] M. Jayasree, R. Aparna, R. Anjana, J.A. Devi, N. John, K. Abha, A. Manikandan, S. George, Fluorescence turn on detection of bilirubin using Fe (III) modulated BSA stabilized copper nanocluster; a mechanistic perception, Analytica chimica acta, 1031 (2018) 152-160.
[25] R. Anjana, J.A. Devi, M. Jayasree, R. Aparna, B. Aswathy, G. Praveen, G. Lekha, G. Sony, S, N-doped carbon dots as a fluorescent probe for bilirubin, Microchimica Acta, 185 (2018) 11.
[26] K. Shanmugaraj, S.A. John, Water-soluble MoS2 quantum dots as effective fluorescence probe for the determination of bilirubin in human fluids, Spectrochimica Acta Part A: Molecular and Biomolecular Spectroscopy, 215 (2019) 290-296.
[27] C. Lu, J.-M. Lin, C.W. Huie, Determination of total bilirubin in human serum by chemiluminescence from the reaction of bilirubin and peroxynitrite, Talanta, 63 (2004) 333-337.
[28] I.I. Timofeeva, C.S. Vakh, A.V. Bulatov, P.J. Worsfold, Flow analysis with chemiluminescence detection: Recent advances and applications, Talanta, 179 (2018) 246-270.
[29] J. Klemm, M.I. Prodromidis, M.I. Karayannis, An enzymic method for the determination of bilirubin using an oxygen electrode, Electroanalysis: An International Journal Devoted to Fundamental and Practical Aspects of Electroanalysis, 12 (2000) 292-295.
[30] H. Sun, Z. Nie, Y.S. Fung, Determination of free bilirubin and its binding capacity by hsa using a microfluidic chip- capillary electrophoresis device with a multi- segment circular-ferrofluid- driven micromixing injection, Electrophoresis, 31 (2010) 3061-3069.
[31] Q. Feng, Y. Du, C. Zhang, Z. Zheng, F. Hu, Z. Wang, C. Wang, Synthesis of the multi-walled carbon nanotubes-COOH/graphene/gold nanoparticles nanocomposite for simple determination of Bilirubin in human blood serum, Sensors and Actuators B: Chemical, 185 (2013) 337-344.
[32] N. Chauhan, R. Rawal, V. Hooda, U. Jain, Electrochemical biosensor with graphene oxide nanoparticles and polypyrrole interface for the detection of bilirubin, Rsc Advances, 6 (2016) 63624-63633.
[33] M. Santhosh, S.R. Chinnadayyala, N.K. Singh, P. Goswami, Human serum albumin-stabilized gold nanoclusters act as an electron transfer bridge supporting specific electrocatalysis of bilirubin useful for biosensing applications, Bioelectrochemistry, 111 (2016) 7-14.
[34] C. Zhang, F. Zhao, Y. She, S. Hong, X. Cao, L. Zheng, S. Wang, T. Li, M. Wang, M. Jin, A disposable molecularly imprinted sensor based on Graphe@ AuNPs modified screen-printed electrode for highly selective and sensitive detection of cyhexatin in pear samples, Sensors and Actuators B: Chemical, 284 (2019) 13-22.
[35] M. Akhoundian, T. Alizadeh, M.R. Ganjali, P. Norouzi, Ultra-trace detection of methamphetamine in biological samples using FFT-square wave voltammetry and nano-sized imprinted polymer/MWCNTs-modified electrode, Talanta, 200 (2019) 115-123.
[36] Q. Yang, X. Wu, H. Peng, L. Fu, X. Song, J. Li, H. Xiong, L. Chen, Simultaneous phase-inversion and imprinting based sensor for highly sensitive and selective detection of bisphenol A, Talanta, 176 (2018) 595-603.
[37] T. Alizadeh, M. Akhoundian, M.R. Ganjali, An innovative method for synthesis of imprinted polymer nanomaterial holding thiamine (vitamin B1) selective sites and its application for thiamine determination in food samples, Journal of Chromatography B, 1084 (2018) 166-174.
[38] M. Akhoundian, T. Alizadeh, M.R. Ganjali, F. Rafiei, A new carbon paste electrode modified with MWCNTs and nano-structured molecularly imprinted polymer for ultratrace determination of trimipramine: The crucial effect of electrode components mixing on its performance, Biosensors and Bioelectronics, 111 (2018) 27-33.
[39] M. Beytur, F. Kardaş, O. Akyıldırım, A. Özkan, B. Bankoğlu, H. Yüksek, M.L. Yola, N. Atar, A highly selective and sensitive voltammetric sensor with molecularly imprinted polymer based

silver@ gold nanoparticles/ionic liquid modified glassy carbon electrode for determination of ceftizoxime, Journal of Molecular Liquids, 251 (2018) 212-217.
[40] N. Özcan, H. Medetalibeyoglu, O. Akyıldırım, N. Atar, M.L. Yola, Electrochemical detection of amyloid-β protein by delaminated titanium carbide MXene/multi-walled carbon nanotubes composite with molecularly imprinted polymer, Materials Today Communications, 23 (2020) 101097.
[41] L. Chen, X. Wang, W. Lu, X. Wu, J. Li, Molecular imprinting: perspectives and applications, Chemical Society Reviews, 45 (2016) 2137-2211.
[42] M.L. Yola, N. Atar, Development of molecular imprinted sensor including graphitic carbon nitride/N-doped carbon dots composite for novel recognition of epinephrine, Composites Part B: Engineering, 175 (2019) 107113.
[43] C.P. Böke, O. Karaman, H. Medetalibeyoglu, C. Karaman, N. Atar, M.L. Yola, A new approach for electrochemical detection of organochlorine compound lindane: Development of molecular imprinting polymer with polyoxometalate/carbon nitride nanotubes composite and validation, Microchemical Journal, 157 (2020) 105012.
[44] Z. Jiang, G. Li, M. Zhang, A novel sensor based on bifunctional monomer molecularly imprinted film at graphene modified glassy carbon electrode for detecting traces of moxifloxacin, RSC advances, 6 (2016) 32915-32921.
[45] R.S. Gomes, F.T. Moreira, R. Fernandes, M.G.F. Sales, Sensing CA 15-3 in point-of-care by electropolymerizing O-phenylenediamine (oPDA) on Au-screen printed electrodes, PloS one, 13 (2018) e0196656.
[46] J. Lee, E. Garon, D. Wong, Salivary diagnostics, Orthodontics & craniofacial research, 12 (2009) 206-211.
[47] V. Pathiyil, R. Udayasankar, Salivary Diagnostics, Saliva and Salivary Diagnostics, IntechOpen, 2019.
[48] M.A. Beluomini, J.L. da Silva, G.C. Sedenho, N.R. Stradiotto, D-mannitol sensor based on molecularly imprinted polymer on electrode modified with reduced graphene oxide decorated with gold nanoparticles, Talanta, 165 (2017) 231-239.
[49] S. Xiao-Xue, L. Xiu-Qi, W. Xiao-Ping, L. Jian-Ping, Molecularly Imprinted Photoelectrochemical Sensor Based on AgBiS2/Bi2S3 for Determination of Propoxur, Chinese Journal of Analytical Chemistry, 48 (2020) 396-404.
[50] S. Kumaravel, S.-H. Wu, G.-Z. Chen, S.-T. Huang, C.-M. Lin, Y.-C. Lee, C.-H. Chen, Development of ratiometric electrochemical molecular switches to assay endogenous formaldehyde in live cells, whole blood and creatinine in saliva, Biosensors and Bioelectronics, 171 (2020) 112720.
[51] F. Lopes, J.G. Pacheco, P. Rebelo, C. Delerue-Matos, Molecularly imprinted electrochemical sensor prepared on a screen printed carbon electrode for naloxone detection, Sensors and Actuators B: Chemical, 243 (2017) 745-752.
[52] K. Kor, K. Zarei, Development and characterization of an electrochemical sensor for furosemide detection based on electropolymerized molecularly imprinted polymer, Talanta, 146 (2016) 181-187.
[53] Y. Liang, C. Qu, R. Yang, L. Qu, J. Li, Molecularly imprinted electrochemical sensor for daidzein recognition and detection based on poly (sodium 4-styrenesulfonate) functionalized graphene, Sensors and Actuators B: Chemical, 251 (2017) 542-550.
[54] P.R. Solanki, M.K. Patel, M.A. Ali, B. Malhotra, A chitosan modified nickel oxide platform for biosensing applications, Journal of Materials Chemistry B, 3 (2015) 6698-6708.

[55] N. Maleki, S. Kashanian, E. Maleki, M. Nazari, A novel enzyme based biosensor for catechol detection in water samples using artificial neural network, Biochemical engineering journal, 128 (2017) 1-11.
[56] M.-J. Syu, T.-C. Chiu, C.-Y. Lai, Y.-S. Chang, Amperometric detection of bilirubin from a micro-sensing electrode with a synthetic bilirubin imprinted poly (MAA-co-EGDMA) film, Biosensors and Bioelectronics, 22 (2006) 550-557.
[57] C.-Y. Huang, M.-J. Syu, Y.-S. Chang, C.-H. Chang, T.-C. Chou, B.-D. Liu, A portable potentiostat for the bilirubin-specific sensor prepared from molecular imprinting, Biosensors and Bioelectronics, 22 (2007) 1694-1699.
[58] A. Nikolaev, Y.A. Rozhilo, T. Starozhilova, V. Sarnatskaya, L. Yushko, S. Mikhailovskii, A. Kholodov, A. Lobanov, Mathematical Model of Binding of Albumin—Bilirubin Complex to the Surface of Carbon Pyropolymer, Bulletin of experimental biology and medicine, 140 (2005) 365-369.
[59] C. Wang, W. Cai, X. Shao, Determination of bilirubin using near infrared diffuse reflectance spectroscopy with selective concentration on β-cyclodextrin, Journal of Near Infrared Spectroscopy, 24 (2016) 345-352.
[60] A. Aslıhan Avan, S. Aydar, H. Filik, Voltammetric sensing of bilirubin based on nafion/electrochemically reduced graphene oxide composite modified glassy carbon electrode, Current Analytical Chemistry, 11 (2015) 96-103.
[61] M.M. Moein, D. Jabbar, A. Colmsjö, M. Abdel-Rehim, A needle extraction utilizing a molecularly imprinted-sol–gel xerogel for on-line microextraction of the lung cancer biomarker bilirubin from plasma and urine samples, Journal of Chromatography A, 1366 (2014) 15-23.
[62] Z. Yang, C. Zhang, Molecularly imprinted hydroxyapatite thin film for bilirubin recognition, Biosensors and Bioelectronics, 29 (2011) 167-171.
[63] T. Balamurugan, S. Berchmans, Non-enzymatic detection of bilirubin based on a graphene–polystyrene sulfonate composite, RSC Advances, 5 (2015) 50470-50477.
[64] T. Senthilkumar, S. Asha, Selective and sensitive sensing of free bilirubin in human serum using water-soluble Polyfluorene as fluorescent probe, Macromolecules, 48 (2015) 3449-3461.
[65] J. Narang, N. Chauhan, A. Mathur, V. Chaturvedi, C. Pundir, A third generation bilirubin sensor development by using gold nanomaterial as an immobilization matrix for signal amplification, Adv Mater Lett, 6 (2015) 1012-1017.
[66] R. Rawal, N. Chauhan, M. Tomar, V. Gupta, A contrivance based on electrochemical integration of graphene oxide nanoparticles/nickel nanoparticles for bilirubin biosensing, Biochemical Engineering Journal, 125 (2017) 238-245.

Figure Captions

Fig. 1. SEM images of the MWCNT/GCE (A), MIP/MWCNT/GCE (B), MIP/MWCNT/GCE (C), and NIP/MWCNT/GCE (D) after removing the template

Fig. 2. (A) Cyclic voltammograms of the template BR MIP/MWCNT/GCE in the 0.1 M acetate buffer of pH 5 at 50 mV s^{-1} scan rate and 20 number of scans. (B) CVs of MWCNT/GCE (curve-red), NIP/MWCNT/GCE (curve-black), NIP/MWCNT/GCE after washing with acetonitrile/acetic acid (curve-purple), NIP/MWCNT/GCE after rebinding of BR (1 fM). (curve-blue). (C) CVs of the GCE (curve-black), MWCNT/GCE (curve-red), MIP/MWCNT/GCE (curve-blue), MIP/MWCNT/GCE after washing with acetonitrile/acetic acid (curve-purple), MIP/MWCNT/GCE after rebinding of BR (1 fM). (curve-green). (D) Nyquist plots obtained at GCE (curve-purple), MWCNT/GCE (curve-black), MIP/MWCNT/GCE (curve-red), MIP/MWCNT/GCE after template removal (curve-blue).

Fig. 3. Solvent effect in washing analyte from the electrode surface (A). Effect of pH of working solution on BR adsorption in MIP cavities in PBS buffer solution (B). Influence of incubation time on the response of the MIP/MWCNT/GCE sensor in PBS (pH 7.0). (C).

Fig. 4. Effect of different molar ratios of BR to functional monomer on the current response (A). Effect of different electropolymerization scan cycles on the current response (B).

Fig. 5. Cyclic voltammograms of MIP/MWCNT/GCE at different scan rates. The inset of figure is the anodic and the cathodic peak currents versus square-root of scan rate plot.

Fig. 6. Calibration curves for BR detection using MIP/MWCNT/GCE in 10 mM $[Fe(CN)_6]^{3-/4-}$ after 10 min of rebinding in PBS under pH 7.

Fig. 7. The current responses for BR and other structural analogs on MIP sensor and NIP sensor. Error bars are standard deviations across three repetitive experiments.

Table Captions

Table 1. Comparison of detection limit and linear range of several methods with the proposed BR detection sensor

Table 2. Comparison of recovery results related to the detection of bilirubin in human serum and saliva (n=4)

Table 3. Analysis and comparing the results of real samples with the method performed in this work and the reference method (n=4)

Figure

Click here to access/download;Figure;Graphical Abstract (3).jpg

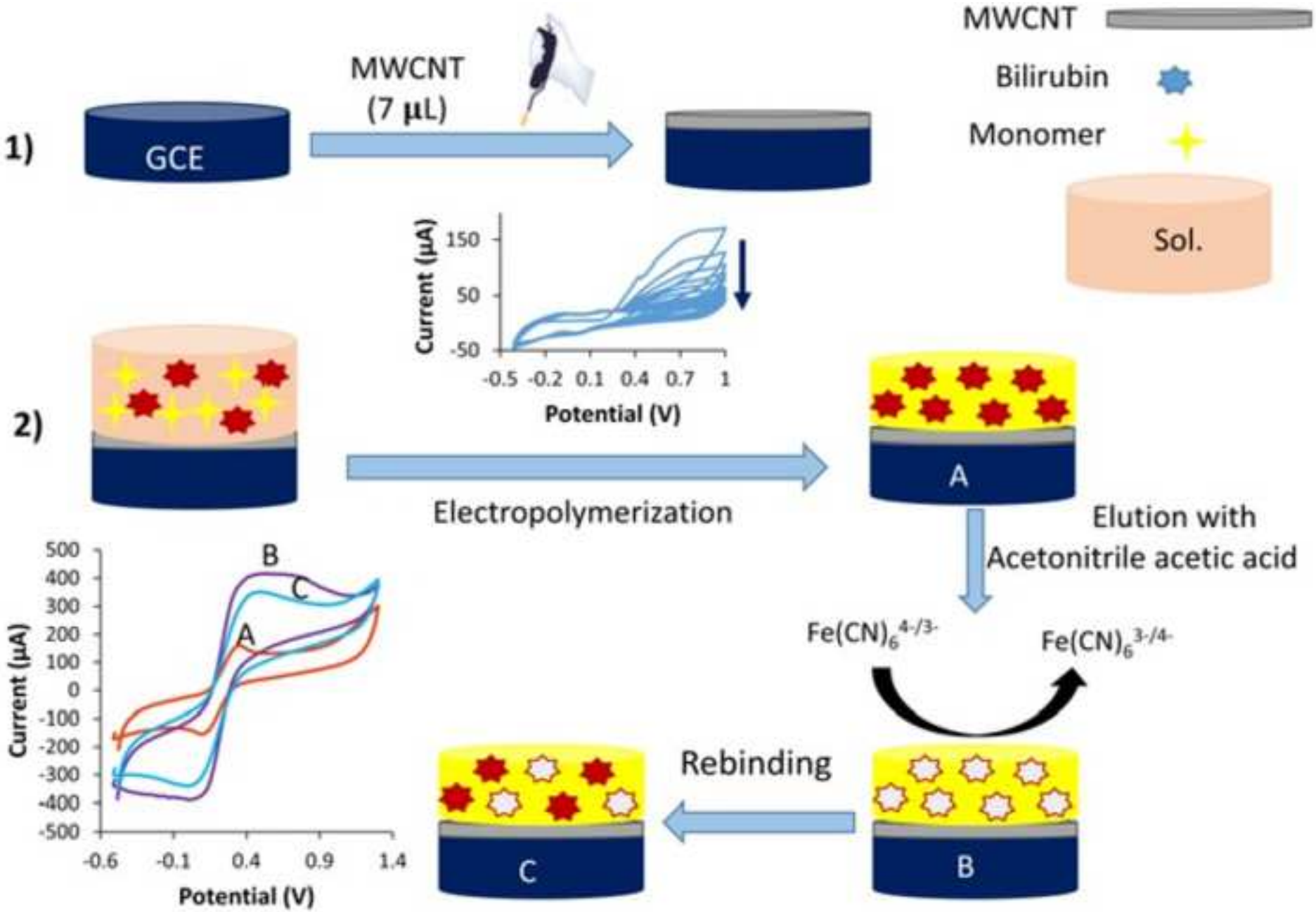

Graphical Abstract

Figure

Click here to access/download;Figure;Figure 1.jpg

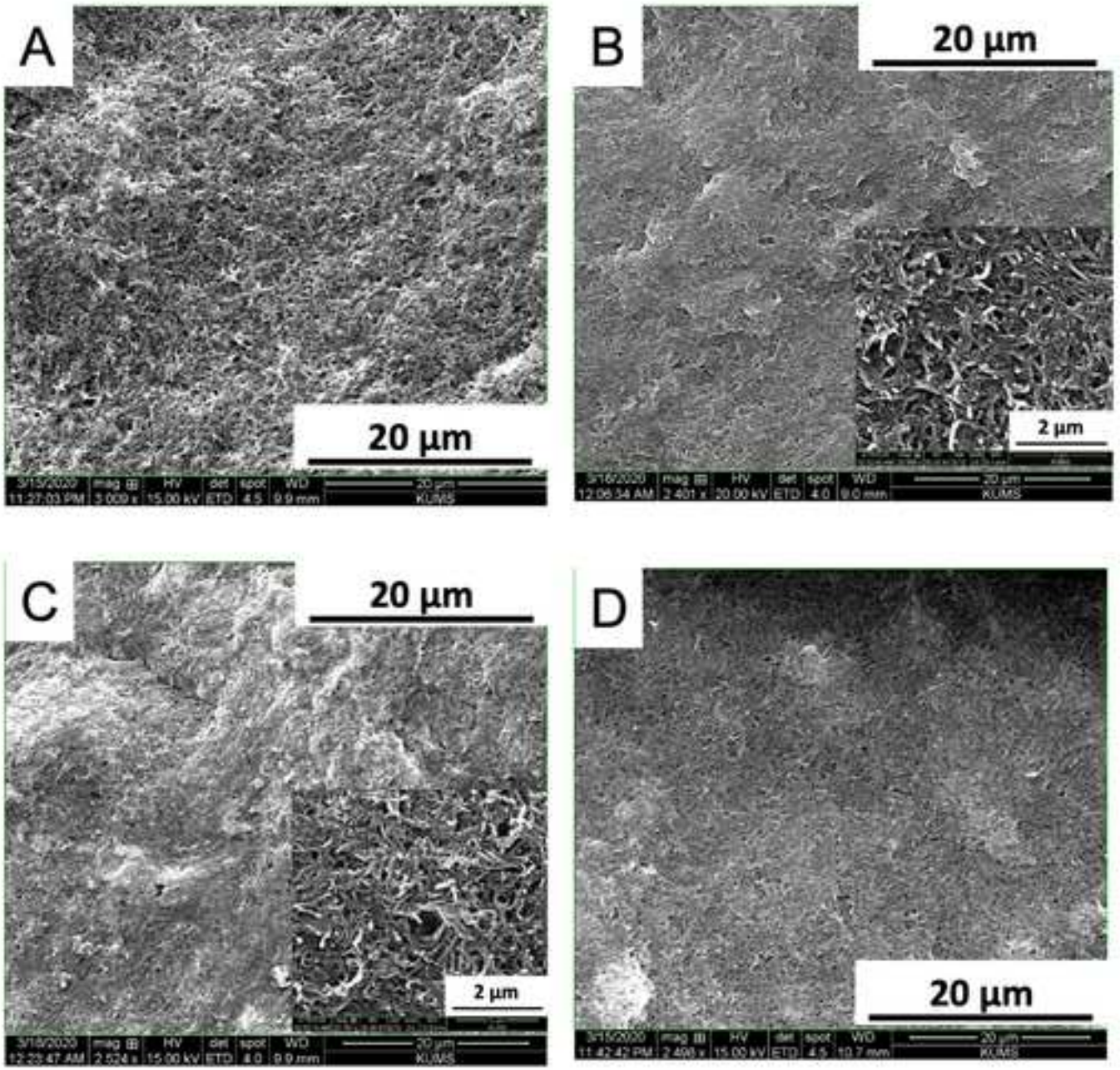

Figure 1

Figure

Click here to access/download;Figure;Figure 2.jpg

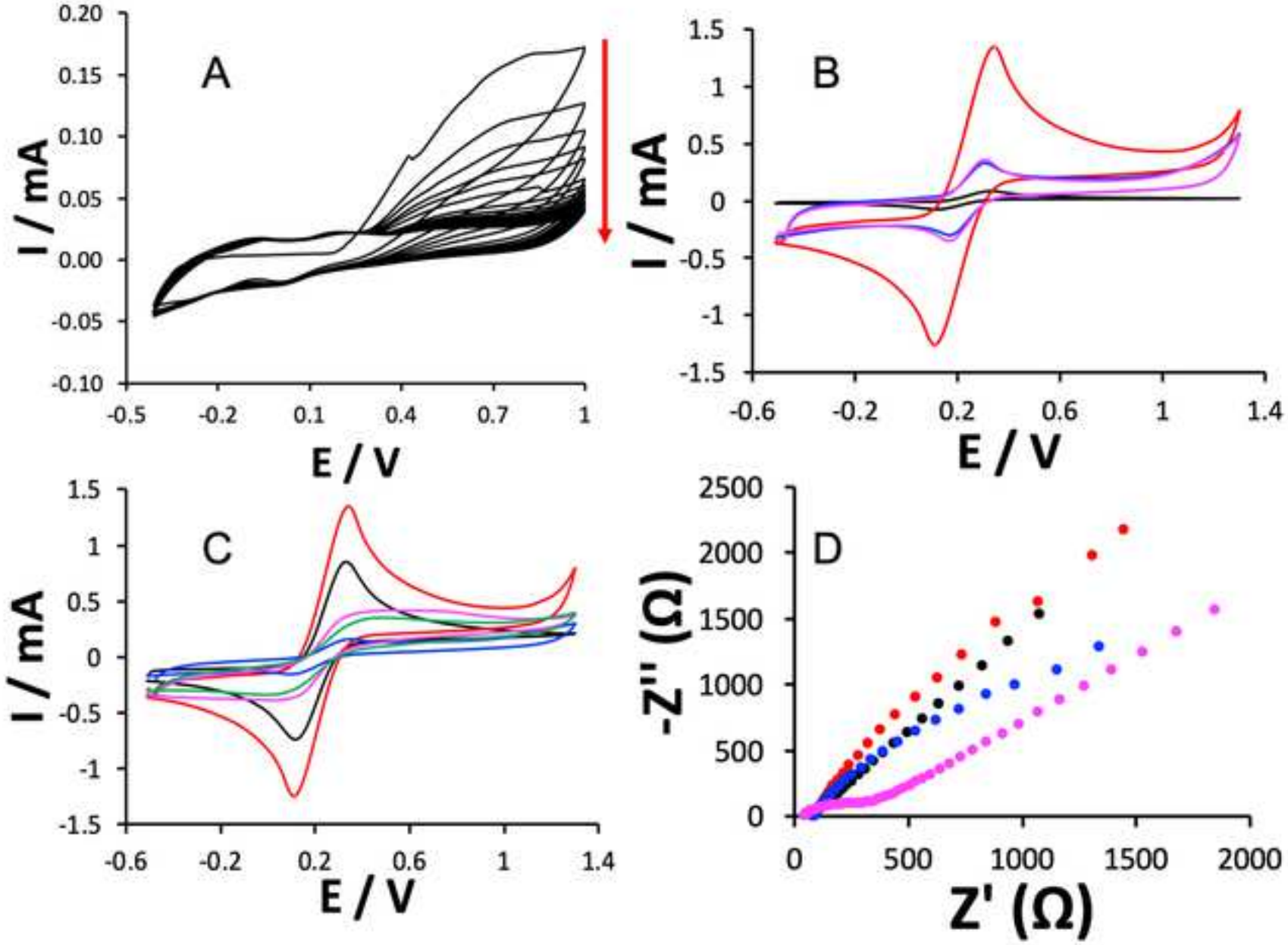

Figure 2

Figure

Click here to access/download;Figure;Figure 3.jpg

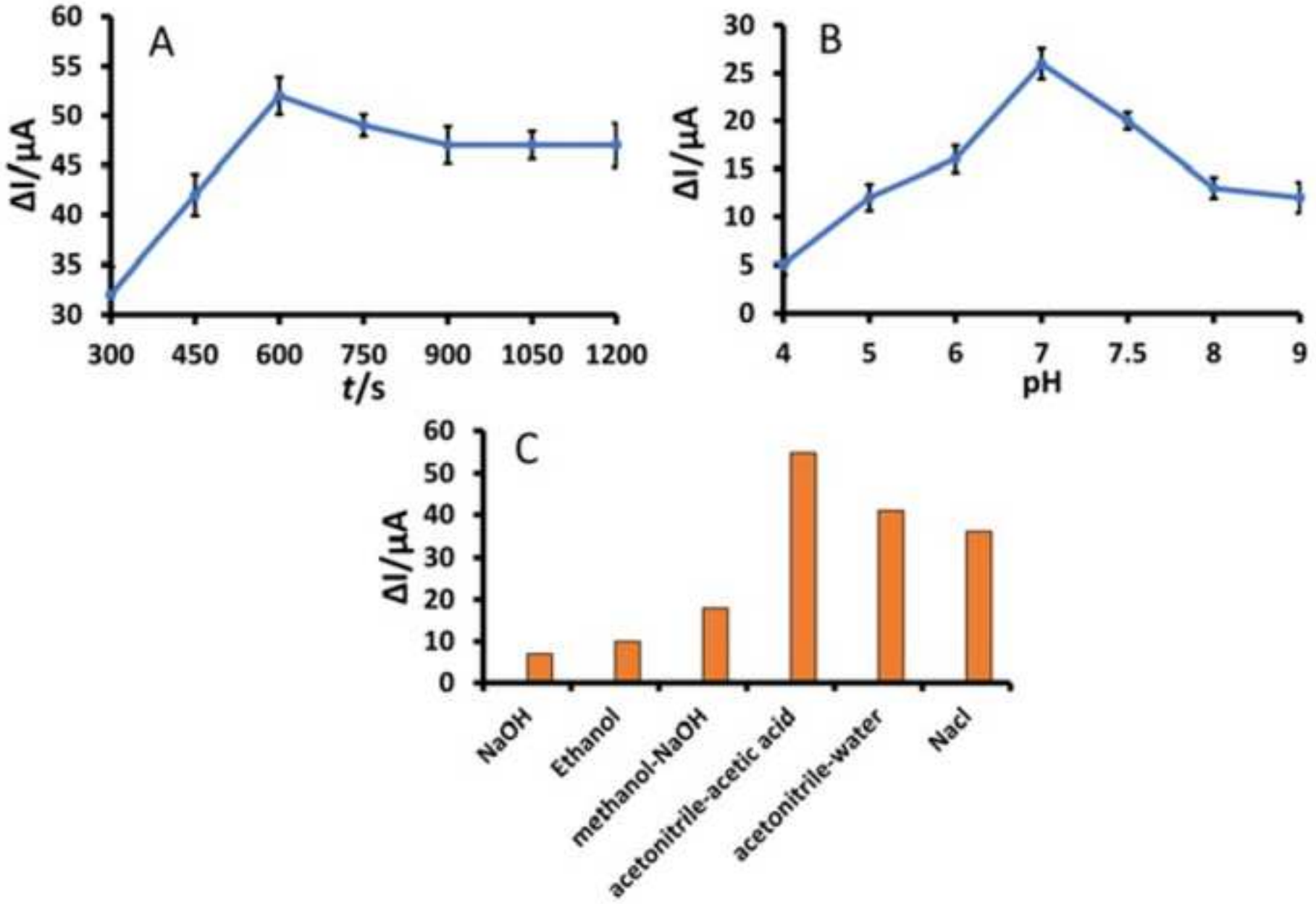

Figure 3

Figure

Click here to access/download;Figure;Figure 4.jpg

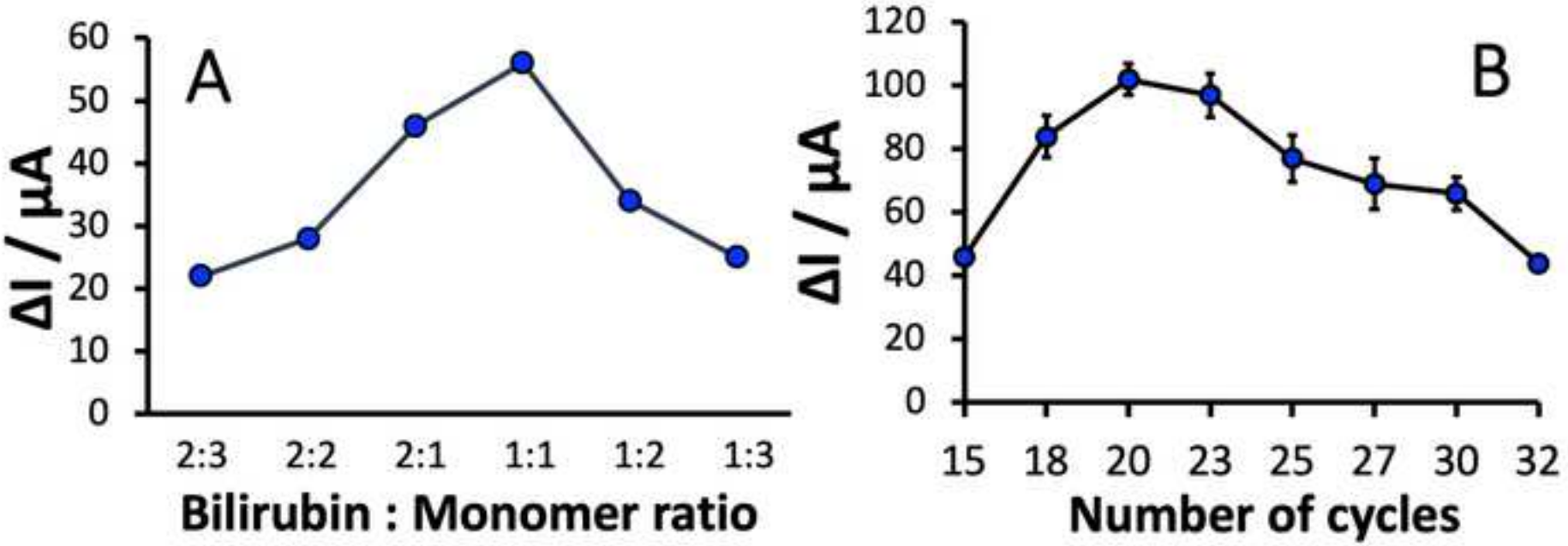

Figure 4

Figure

Click here to access/download;Figure;Figure 5.jpg

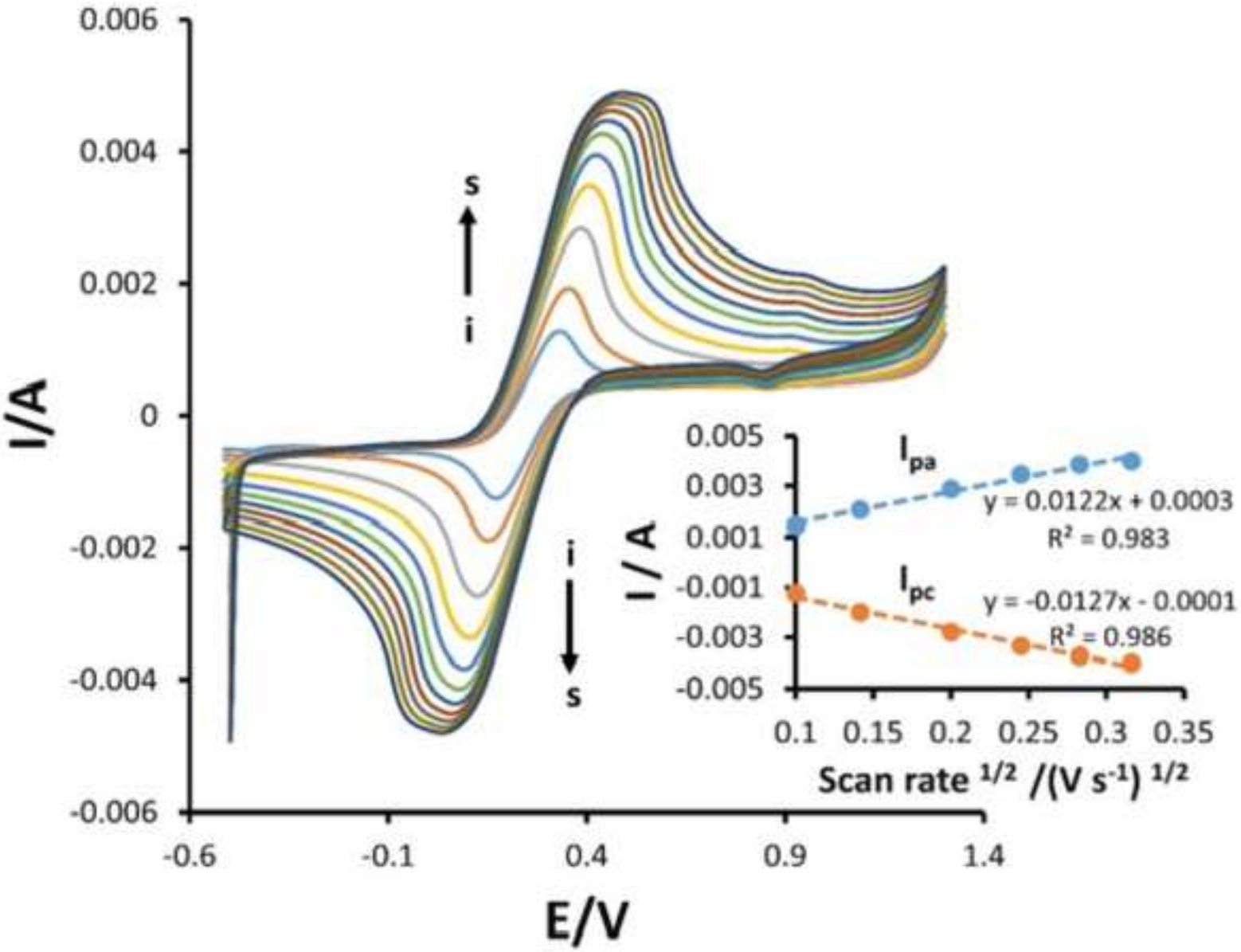

Figure 5

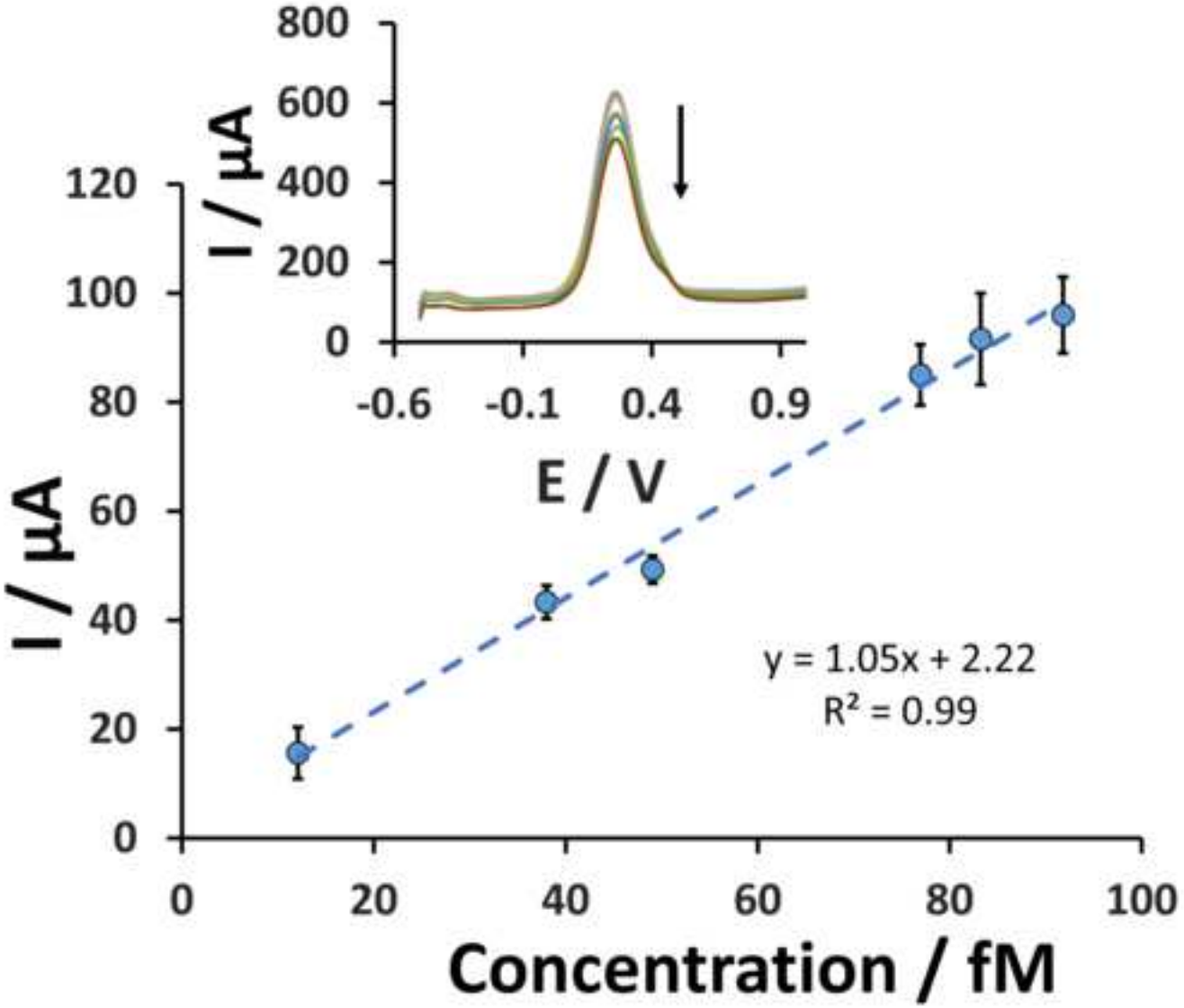

Figure 6

Figure

Click here to access/download;Figure;Figure 7.jpg

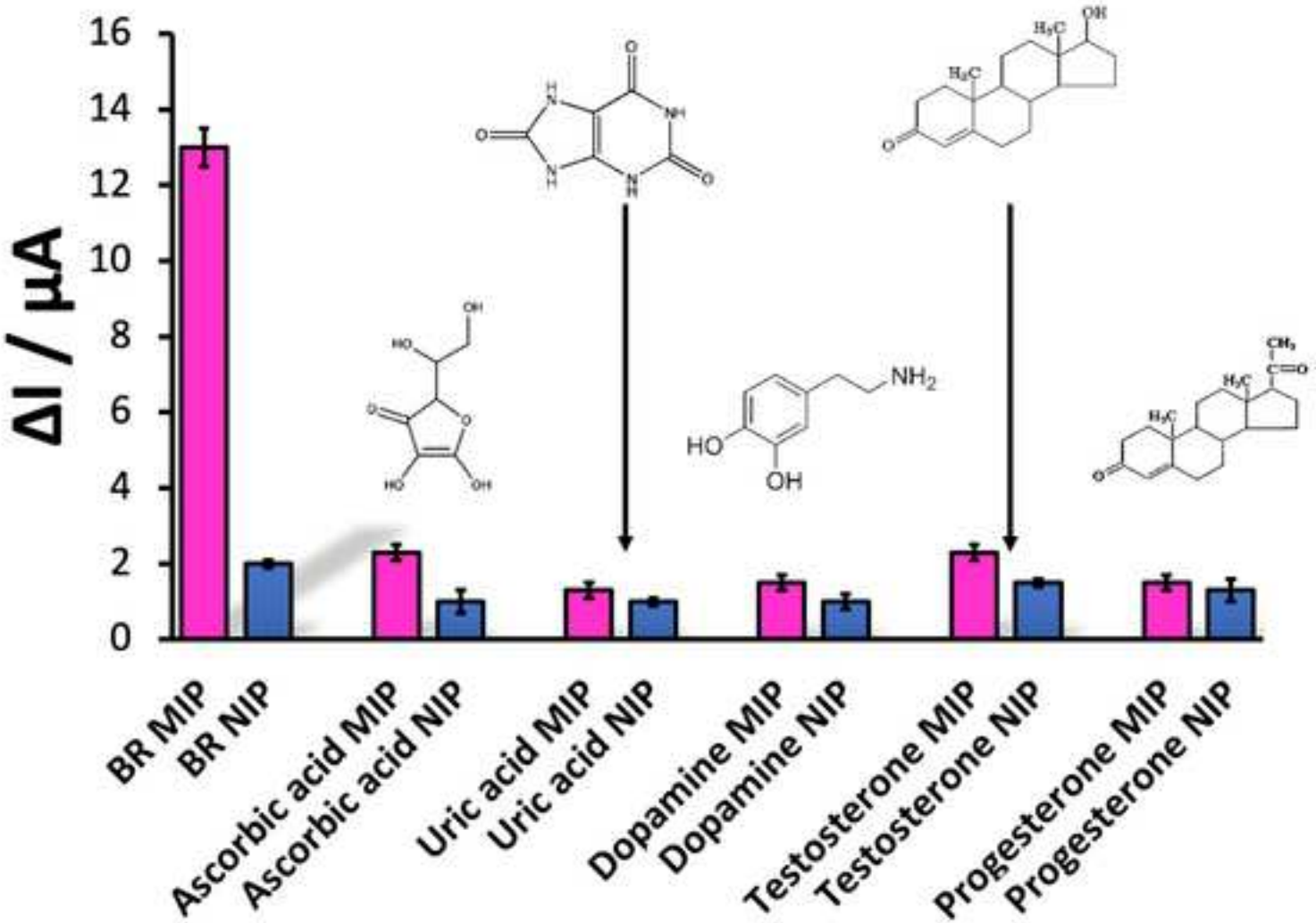

Figure 7

Table 1

Electrode	Detection Method	LOD	Linear Range	Reference
MIP/$H_3PW_{12}O_{40}$/C_3N_4 NTs/GCE	Electrochemical	300 fM	1.0–100 pM	[10]
----------	Near infrared diffuse reflectance spectroscopy (NIR-DRS)	4.4 μM	5.6–15 μM	[59]
Sol-gel IP[a]/MWCNT/CPE	CV	0.75 μM	1–100 μM	[1]
Nafion/RGO[b]/GCE	SWV	0.84 μM	2–70 μM	[60]
Imprinted sol-gel xerogel	Electrochemical	1.6 nM	5–1000 nM	[61]
Bilirubin-imprinted hydroxyapatite film	Quartz crystal microbalance (QCM)	0.01 μM	0.05–80 μM	[62]
MIP/POM/CN[c]/GCE	SWV	0.1 pM	1–100 pM	[10]
BOx/GONP/Ppy/FTO[d]	Amperometry	0.1 nM	0.01–500 μM	[32]
RGO/PSS/GCE[e]	Chronoamperometry	2 μM	Up to 450 μM	[63]
Fluoresence quenching of polyfluorene	Fluorimetric	0.15 μM	25-50 μM	[64]
Box/GME[f]	square-wave voltammetry (SWV)	0.005 μM	0.01–500 μM	[65]
Covalently immobilized HSAAuNC over ITO	Amperometric	0.085 μM	0.2–7 μM	[33]

Box/GrONPs/NiNPs/ITO[g]	Amperometry	0.15 nM	0.01–600 μM	[66]
OPD/MWCNT/GCE	Electrochemical	7.8 fM	12.1-91.8 f M	This work

a: Imprinted polymer **b**: Reduced graphene oxide, **c**: Polyoxometalate/Carbon Nitride Nanotubes, **d**: Bilirubin oxidase/graphene oxide nanoparticles/polypyrrole/fluorine doped tin oxide glass plate, **e**: Reduced graphene oxide/poly styrene sulfonate/glassy carbon electrode, **f**: Bilirubin oxidase/gold microelectrode, **g**: Bilirubin oxidase/graphene oxide nanoparticles/nickel nanoparticles/ITO.

Table 2

Sample	Dilution of Sample	Added concentration (nM)	Found (nM)	Recovery (%)	[a]RSD (n=4)
Serum	1000 times dilution	10	9.78	97.85	6.28
		15	14.66	97.77	3.39
		20	19.04	95.23	3.88
	10,000 times dilution	10	10.38	103.80	1.90
		15	14.42	96.19	1.21
		20	19.71	98.57	1.82
Saliva	0 dilution	10	9.95	99.5	4.93
		15	14.11	94.07	4.86
		20	19.71	98.57	2.51
	10 times dilution	10	9.97	99.76	3.5
		15	13.92	92.85	3.08
		20	19.88	99.40	5.1
	100 times dilution	10	10.22	102.21	1.67
		15	14.35	95.71	1.96
		20	18.48	92.41	6.3
	1000 times dilution	10	9.91	99.16	4.73
		15	14.76	98.46	3.63
		20	19.35	96.78	3.75

Table 3. Analyze and compare the results of real samples with the method performed in this work and the reference method (n=4)

Saliva							Serum						
Method	**Detected (µM)**	**Sample**	**Added (µM)**	**Found (µM)**	**Recovery (%)**	**RSD (n=4)**	**Method**	**Detected (10^{-5})**	**Sample**	**Added (10^{-5})**	**Found (10^{-5})**	**Recovery (%)**	**RSD (n=4)**
HPLC	7.2	**Sample 1**	_	7.02	97.55	6.3	**Fluorometer kit**	22.2	**Sample 1**	_	20.47	92.23	2.47
		Sample 2	0.1	7.07	96.86	4.9			**Sample 2**	0.1	20.59	92.35	2.04
		Sample 3	0.3	7.09	94.60	6.9			**Sample 3**	0.3	22.26	98.94	7.60
		Sample 4	0.6	7.61	92.95	5.9			**Sample 4**	0.6	22.14	97.11	2.08